

My Thesis Title

Matthew Lawrence Joyce

August 14, 2020

CONTENTS

1.	<i>The Standard Model</i>	5
2.	<i>Supersymmetry</i>	6
3.	<i>The Large Hadron Collider</i>	7
3.1	Introduction	7
3.2	Injection Complex	7
3.3	Tunnel and Magnets	8
3.4	Luminosity	10
4.	<i>Compact Muon Solenoid</i>	12
4.1	Introduction	12
4.2	Coordinate System	13
4.3	Tracker	14
4.3.1	Pixel Detector	14
4.3.2	Strip Detector	15
4.4	Electromagnetic Calorimeter	16
4.4.1	Crystals	17
4.4.2	Barrel and Endcaps	17
4.4.3	Preshower layer	19
4.4.4	Performance	19
4.5	Hadronic Calorimeter	20
4.6	Muon System	20
5.	<i>MIP Timing Detector</i>	21
5.0.1	Barrel Timing Layer	22

LIST OF FIGURES

3.1	LHC interaction points	8
3.2	Layout of LHC accelerator complex [9].	9
3.3	Proton bunch capture onto RF bucket [2].	10
3.4	Cross section of LHC dipole [4]	11
3.5	Integrated luminosity delivered by the LHC to the CMS experiment each year from 2010-2018.	11
4.1	Schematic of CMS detector [10]	12
4.2	Transverse slice of the CMS detector[3].	13
4.3	Cross section (side) of CMS tracker prior to the Phase 1 upgrade during the year-end technical stop of 2016/2017. Each line represents a detector module while double lines indicate back-to-back strip modules. Surrounding the pixel tracker (PIXEL) is the strip detector, which is divided into the Tracker Inner Barrel (TIB), Tracker Outer Barrel (TOB), Tracker Inner Disks (TID), and Tracker Endcaps (TEC). Reprinted from Reference [6].	15
4.4	Cross section (side) of pixel detector. The lower half , labeled "Current", shows the design prior to 2017 while the upper half, labeled "Upgrade", shows the design after the upgrade. Reprinted from Resource [5]	16
4.5	PbWO ₄ crystals. Left: EB crystal with APD. Right: EE crystal with VPT. Reprinted from [7]	18
4.6	Schematic of ECAL. Reprint from [7]	19
5.1	Timeline for LHC	21
5.2	Timelayer thingy	22

LIST OF TABLES

4.1 Summary of signals expected for each particle type in each sub-detector	13
--	----

1. THE STANDARD MODEL

2. SUPERSYMMETRY

3. THE LARGE HADRON COLLIDER

3.1 *Introduction*

The Large Hadron Collider (LHC) is a 26.7 kilometer-long, two-ring particle accelerator and collider located on the border of France and Switzerland at the European Organization for Nuclear Research (CERN). During normal operations the LHC maintains two counter-rotating beams of proton bunches that collide at four interaction points (IP) with up to $\sqrt{s} = 14$ TeV center of mass energy and a luminosity of $10^{34}\text{cm}^{-2}\text{s}^{-1}$. The ALICE (Point 2), ATLAS (Point 1), CMS (Point 5), and LHC-b experiments each have a detector at one of these interaction points as seen in Figure 3.1 . The CMS and ATLAS are general-purpose detectors while LHC-b specializes in beauty quark studies. ALICE is a heavy-ion experiment which uses $^{208}\text{Pb} - p$ or $^{208}\text{Pb} - ^{208}\text{Pb}$ collisions that can also be produced by the LHC.

3.2 *Injection Complex*

In order to bring the protons from rest up to their target collision energy a series of accelerators, as shown in Figure 3.2, are used. The acceleration sequence begins with the injection of hydrogen gas into a duoplasmatron. Here a bombardment of electrons ionize the hydrogen atoms while an electric field pushes them through the duoplasmatron cavity. The result is 100 keV protons being passed on to a quadrupole magnet which guides them into the aperture of a linear accelerator (LINAC2). The radio frequency (RF) cavities in LINAC2 accelerate the protons up to 50 MeV. At this point the protons are sent into one of four rings in the Proton Synchrotron Booster (PSB). The PSB repeatedly accelerates the protons around a circular path until they reach an energy of 1.4 GeV. The bunches of protons from each PSB ring are then sequentially injected into the single-ringed Proton Synchrotron (PS). Each bunch injected into the PS are captured by one of the "buckets" (Figure 3.3) provided by the PS RF system which also manipulates the bunches into the desired profile and proton density. These proton bunches are accelerated to 25 GeV and injected into the Super Proton Synchrotron

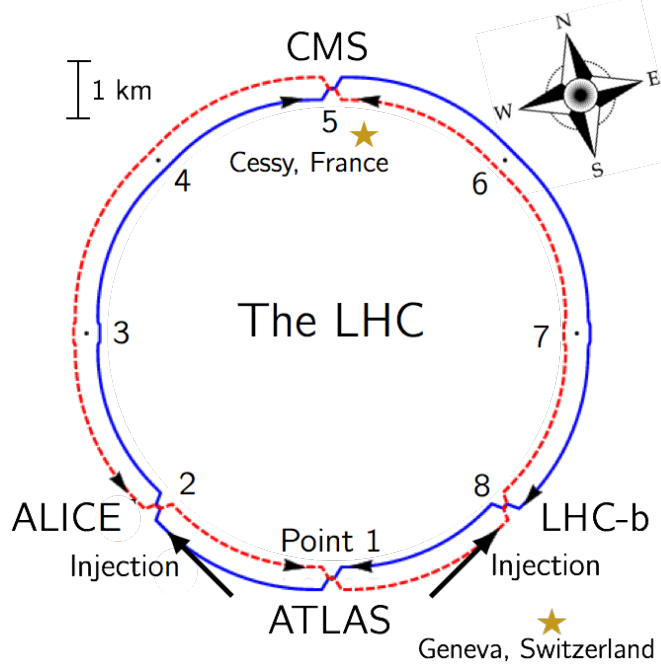


Fig. 3.1: Interaction points of the LHC

(SPS) where they are accelerated to 450 GeV. Finally the proton bunches are injected into the LHC ring where they are accelerated to 6.5 TeV and collided in 25 ns intervals to yield a center of mass energy of $\sqrt{s} = 13$ TeV.

3.3 Tunnel and Magnets

The LHC was designed to produce collisions with up to $\sqrt{s} = 14$ TeV. That requires confining and guiding 7 TeV protons around the circumference of the LHC ring. The ring is housed in a 4 meter-wide underground tunnel that ranges in depth between 45 and 170 meters below the surface. This tunnel was repurposed from the Large Electron-Positron (LEP) Collider which previously occupied the space. For this reason the tunnel is not completely circular but is instead made up of alternating curved and straight sections of 2500 m and 530 m in length respectively. The straight sections, labeled 1-8 in Figure 3.1, are used as either experimental facilities or sites for hardware necessary for LHC operations such as RF cavities for momentum cleaning, quadrupole magnets for beam focusing, and sextupole magnets for acceleration and betatron cleaning.

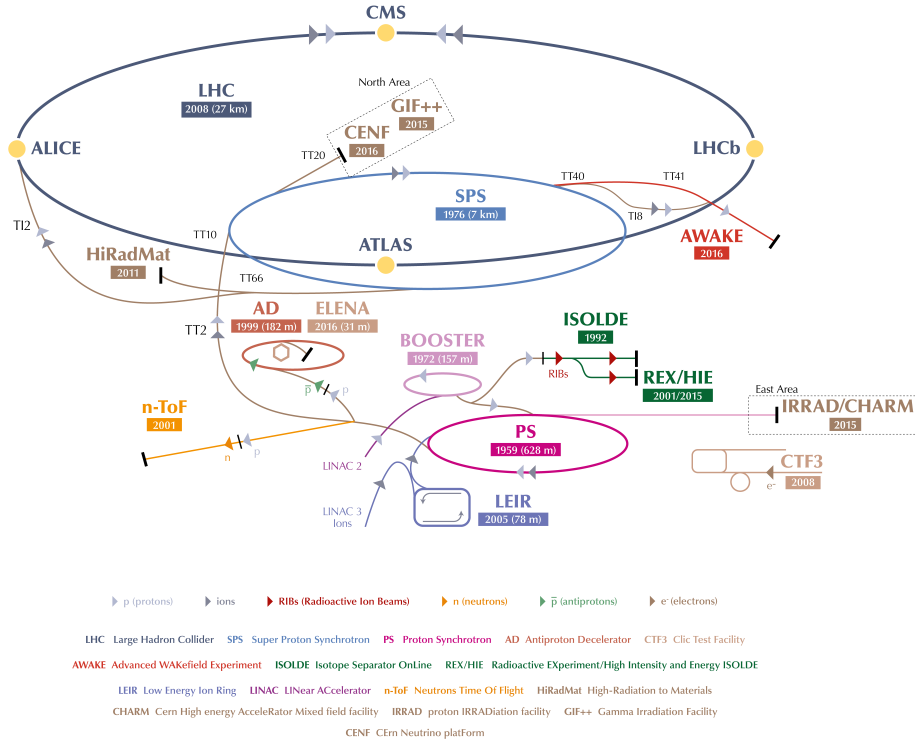


Fig. 3.2: Layout of LHC accelerator complex [9].

Steering a 7 TeV proton beam around the curved sections requires a magnetic field of 8.33 Tesla which is provided by 1223 superconducting dipole magnets cooled to 1.9 K. A cross section of the LHC dipole is shown in Figure 3.4. Supercooled liquid helium flows through the heat exchanger pipe to cool the iron yolk to a temperature of 1.9 K. Ultra high vacuum is maintained in the outer volume to provide a layer of thermal insulation between the inner volume and the outer steel casing. Inside the iron yolk is a twin bore assembly of niobium-titanium superconducting coils. Two parallel beam pipes are located within the focus of the superconducting coils. This is the ultra high vacuum region where the subatomic particles are confined as they travel around the LHC ring.

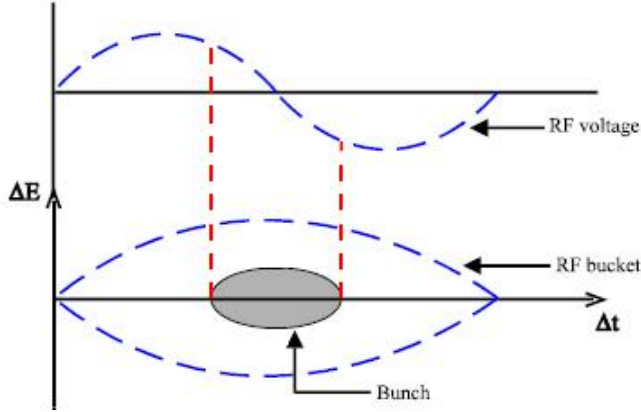


Fig. 3.3: Proton bunch capture onto RF bucket [2].

3.4 Luminosity

The number of events generated per second for specific process having cross-section σ_{event} is given by:

$$\frac{dN_{event}}{dt} = L\sigma_{event} \quad (3.1)$$

where L is the machine luminosity. The machine luminosity for a Gaussian beam distribution can be written in terms of the beam parameters as:

$$L = \frac{N_b^2 n_b f_{rev} \gamma_r}{4\pi \epsilon_n \beta_*} F \quad (3.2)$$

where N_b is particle density in each bunch, n_b is the number of bunches in each beam, f_{rev} is the frequency of revolution, and γ_r is the relativistic gamma factor. The variables ϵ_n and β_* are the normalized transverse beam emittance and the beta function at the IP respectively, while F is the geometric reduction factor depending due to the beams' crossing angle at the IP. [9]

The total number of events produced over a given amount of time would then be

$$N_{event} = \sigma_{event} \int L dt = \sigma_{event} L_{integrated}. \quad (3.3)$$

The integrated luminosity delivered each year to the CMS experiment is shown in 3.5. The analysis presented here uses data collected from the 2016, 2017, and 2018 campaigns which gives a combined integrated luminosity of 158.7 fb^{-1} .

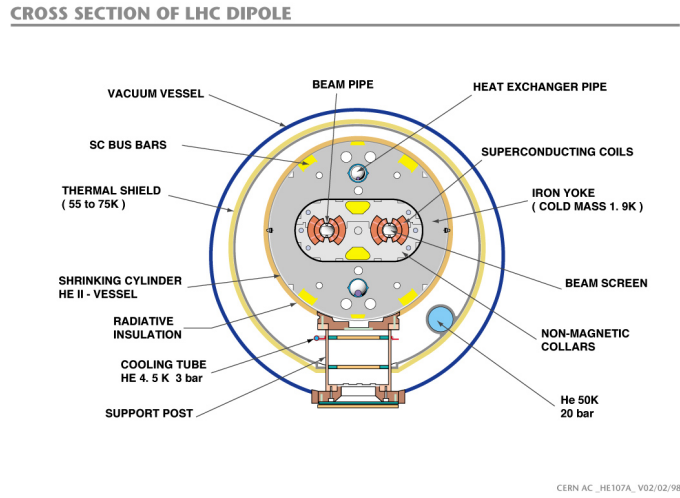


Fig. 3.4: Cross section of LHC dipole [4]

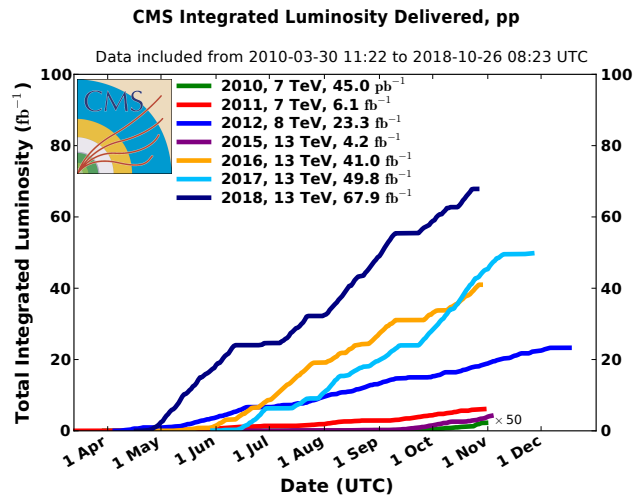


Fig. 3.5: Integrated luminosity delivered by the LHC to the CMS experiment each year from 2010-2018.

4. COMPACT MUON SOLENOID

4.1 Introduction

About 100 meters below the town of Cessy, France at Point 5 is the Compact Muon Solenoid (CMS). The CMS is a general purpose detector weighing 14,000 tonnes with a length of 28.7 meters and a 15.0-meter diameter that was designed to accurately measure the energy and momentum of particles produced in the proton-proton or heavy-ion collisions at the LHC [7]. A perspective view of the detector is shown in Figure 4.1. In order to get a full picture of what is being produced by the collisions the CMS detector must be able identify the resulting particles as well as accurately measure their energy and momentum. For this reason the detector was designed to be a collection of specialized sub-detectors, each of which contributes data used in the reconstruction of a collision.

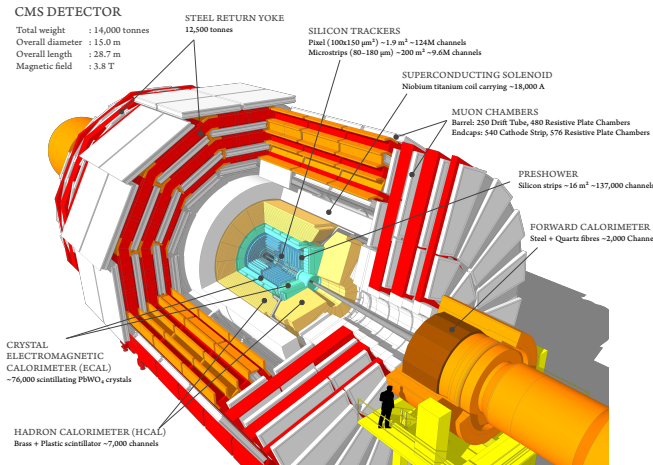


Fig. 4.1: Schematic of CMS detector [10]

At the heart of the CMS detector is a 3.8-Tesla magnetic field produced by a superconducting solenoid. Inside the 6-meter diameter solenoid are

three layers of sub-detectors. These make up the inner detector and are, in order from innermost to outermost, the silicon tracker, the electromagnetic calorimeter (ECAL), and the hadronic calorimeter (HCAL). Outside the solenoid is the muon system. A transverse slice of the detector (Figure 4.2) shows the sub-detectors and how different types of particles interact with them. Table 4.1 shows a summary of which sub-detectors are expected to produce signals for different types of particles.

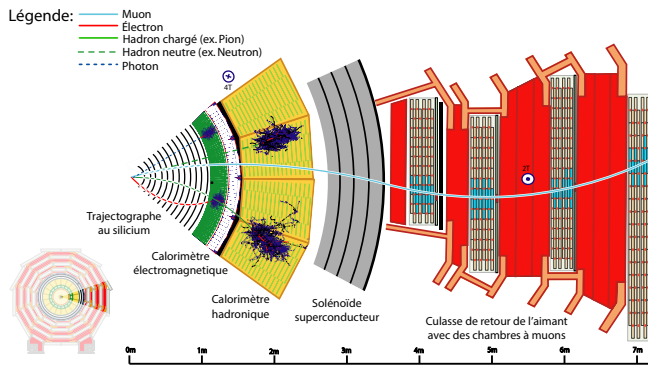


Fig. 4.2: Transverse slice of the CMS detector[3].

Particle	Tracker	ECAL	HCAL	Muon
Photons	No	Yes	No	No
Electrons	Yes	Yes	No	No
Hadrons (charged)	Yes	Yes	Yes	No
Hadrons (neutral)	No	No	Yes	No
Muons	Yes	No	No	Yes
Invisible (ν , SUSY, etc)	No	No	No	No

Tab. 4.1: Summary of signals expected for each particle type in each sub-detector

4.2 Coordinate System

The origin of the coordinate system used by CMS is centered at the nominal collision point in the center of the detector. A right-handed Cartesian system is used with the x-axis pointing radially inward toward the center of the LHC ring, y-axis pointing vertically upward, and the z-axis pointing tangent to

the LHC ring in the counterclockwise direction as viewed from above. CMS also uses an approximately Lorentz invariant spherical coordinate system spanned by three basis vectors. They are the transverse momentum p_T , pseudorapidity η , and azimuthal angle ϕ . The transverse momentum and azimuthal angle translate to the Cartesian system in the following ways using the x and y-components of the linear momentum:

$$p_T = \sqrt{(p_x)^2 + (p_y)^2} \quad (4.1)$$

$$\phi = \tan^{-1} \frac{p_y}{p_x} \quad (4.2)$$

while the pseudorapidity can be translated using the polar angle θ relative the positive z-axis as

$$\eta = -\ln[\tan \frac{\theta}{2}] \quad (4.3)$$

4.3 Tracker

The innermost sub-detector in CMS is the silicon tracker. The tracker is used to reconstruct tracks and vertices of charged particles. In order to give precise reconstruction of charged particle trajectories it needs to be position as close as possible to the IP and have high granularity. The close proximity to the IP requires the materials to be tolerant to the high levels of radiation in that region. Being the innermost sub-detector it must also minimally disturb particles as they pass through it into the other sub-detectors. These criteria led to the design of the tracker using silicon semiconductors.

The silicon tracker is made up of two subsystems, an inner pixel detector and an outer strip tracker which are oriented in a cylindrical shape with an overall diameter of 2.4 m and length of 5.6 m centered on the interaction point. Both subsystems consist of barrel and endcap regions which can be seen in Figure 4.3.

4.3.1 Pixel Detector

The pixel detector is the innermost subsystem in the silicon tracker and spans the pseudorapidity range $|\eta| < 2.5$ and is responsible for small impact parameter resolution which is important for accurate reconstruction of secondary vertices [7]. In order to produce these precise measurements a very high granularity is required. In addition to this the proximity to the IP means that one expects there to be high occupancy of the tracker. These constraints are met by using pixels with a cell size of $100 \times 150 \mu\text{m}^2$.

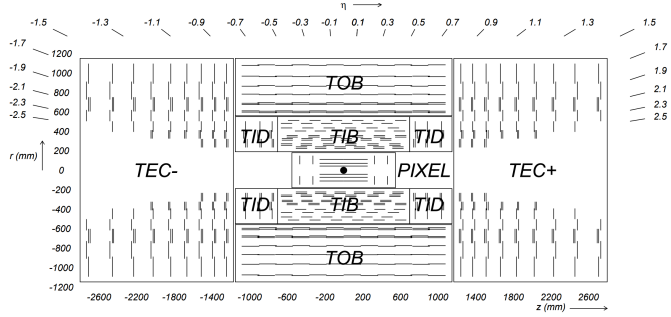


Fig. 4.3: Cross section (side) of CMS tracker prior to the Phase 1 upgrade during the year-end technical stop of 2016/2017. Each line represents a detector module while double lines indicate back-to-back strip modules. Surrounding the pixel tracker (PIXEL) is the strip detector, which is divided into the Tracker Inner Barrel (TIB), Tracker Outer Barrel (TOB), Tracker Inner Disks (TID), and Tracker Endcaps (TEC). Reprinted from Reference [6].

The original pixel detector was designed for operation at the nominal instantaneous luminosity of $10^{34} \text{ cm}^{-2}\text{s}^{-1}$ with 25 ns between proton bunch crossings, resulting in on average about 25 proton-proton interactions occurring per bunch crossing or pileup [6]. During the LHC technical shutdown of 2016/17, the pixel detector underwent the scheduled Phase 1 upgrade which would allow operation at higher levels of instantaneous luminosity and pileup. Figure 4.4 shows a cross sectional view in the r - z plane. Prior to 2017 there were three barrel layers and two endcap layers on each side which provide three very precise space points for each charged particle. The upgrade decreased the radius of the innermost barrel layer from 4.4 cm to 3.0 cm and added a fourth barrel layer as well as adding third endcap layer to each side. Each of the endcap layers consisted of two half-disks populated with pixel modules whereas the upgraded endcap layers were split into inner and outer rings. [5]

4.3.2 Strip Detector

The silicon strip detector surrounds the pixel detector and is comprised of four subsystems, the Tracker Inner Barrel (TIB), the Tracker Outer Barrel (TOB), the Tracker Inner Disks (TID), and the Tracker Endcaps (TEC), all of which can be seen in Figure 4.3 [7]. The TIB and TID both use $320 \mu\text{m}$ thick silicon micro-strip sensors oriented along z and r respectively. The TIB has four layers while the TID is composed of three layers. This

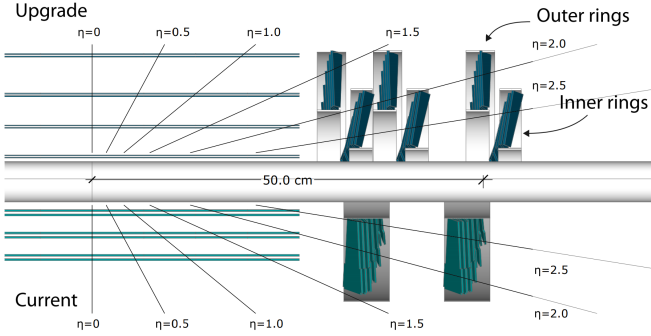


Fig. 4.4: Cross section (side) of pixel detector. The lower half , labeled "Current", shows the design prior to 2017 while the upper half, labeled "Upgrade", shows the design after the upgrade. Reprinted from Resource [5]

geometry allows the TIB and TID to combine to provide up to four $r - \phi$ measurements on charged particle trajectories.

Surrounding the TIB and TID is the TOB, which extends between $z \pm 118$ cm. This subsystem consists of six layers of 500 μm thick silicon micro-strip sensors with strip pitches ranging from 122 μm to 183 μm , providing six more $r - \phi$ measurements in addition to those from the TIB/TID subsystems. Beyond the z range of the TOB is the TEC. Each TEC is made up of nine disks. Each of the nine disks has up to seven concentric rings of micro-strip sensors oriented in radial strips with those on the inner four rings being 320 μm thick and the rest being 500 μm thick, providing up to nine ϕ measurements for the trajectory of a charged particle.

To provide additional measurements of the z coordinate in the barrel and r coordinate in the disks a second micro-strip detector module is mounted back-to-back with stereo angle 100 mrad in the first two layers of the TIB and TOB, the first two rings of the TID, and rings 1, 2, and 5 of the TEC. The resulting single point resolution is 230 μm in the TIB and 530 μm in the TOB. The layout of these subsystems ensures at least nine hits for $|\eta| < 2.4$ with at least four of hits yielding a 2D measurement.

4.4 Electromagnetic Calorimeter

The electromagnetic calorimeter (ECAL) lies just outside the tracker and is a hermetic homogeneous calorimeter designed to measure the energy deposited by electrons and photons. It consists of a central barrel (EB) with 61200 lead tungstate (PbWO_4) crystals which is closed by two endcaps (EE), each

having 7324 crystals. Highly-relativistic charged particles passing through a crystal primarily lose energy by producing bremsstrahlung photons. Photons lose energy by producing $e^- - e^+$ pairs. In front of each EE is a preshower (ES) detector which acts as a two-layered sampling calorimeter. The crystals in the EB are instrumented with avalanche photodiodes (APDs) while the EE crystals are instrumented with vacuum phototriodes (VPTs). The ECAL design was strongly driven to be sensitive to the di-photon decay channel of the Higgs boson. This led to the design of a calorimeter that was fast, radiation-hard, and had good spatial and energy resolution.

4.4.1 Crystals

In order to provide a good spacial resolution it was necessary for the ECAL to have a fine granularity. The small Molier radius (22 mm) and short radiation length (8.9 mm) of PbWO₄ allows for fine granularity while maintaining good energy resolution by containing nearly all of the energy from an EM shower without the need for a restrictively thick crystal layer. The PbWO₄ scintillation is also fast enough that approximately 80 percent of an EM shower is produced within 25 ns, which is the also the amount of time between bunch crossings at the LHC. These crystals have a Gaussian-shaped spectrum spanning from 360 nm to 570 nm with a maximum at approximately 440 nm. While PbWO₄ is relatively radiation-hard, the amount of ionizing radiation seen by the crystal leading up to the HL-LHC era of operations causes wavelength-dependent degradation in light transmission. The scintillation mechanism however is unchanged so this damage can be tracked and accounted for by injecting laser light near the peak wavelength of the emission spectrum into the crystals to monitor optical transparency.

Light produced in the crystal is transmitted along its length and collected at the rear by either an APD in the EB or a VPT in one of the EE. Light output is temperature dependent so the crystals are kept at precisely 18°C at which the yield is about 4.5 photoelectrons per MeV. The EB and EE crystals, which have a tuncated pyramidal shape to match the lateral development of the shower, along with their photosensors are shown in Figure 4.5.

4.4.2 Barrel and Endcaps

The EB covers the pseudorapidity range $|\eta| < 1.479$ and uses crystals that are 230 mm long, which corresponds to 25.8 radiation lengths. The front face of each crystal measures 22×22 mm² while the rear face measures 26×26

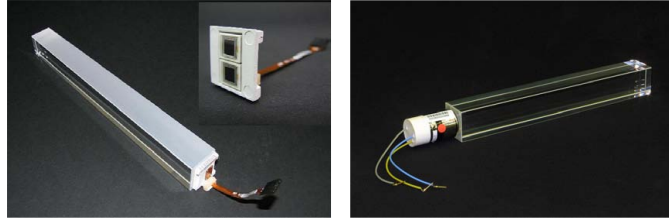


Fig. 4.5: PbWO₄ crystals. Left: EB crystal with APD. Right: EE crystal with VPT. Reprinted from [7]

mm². These are grouped in 36 supermodules (SM), each comprised of 1700 crystals arranged in a 20×85 grid in $\phi \times \eta$. Each SM spans half the length of the barrel and covers 20° in ϕ . On the back face of each crystal is a pair of APDs (semiconductor diodes). APDs are compact, immune to the longitudinal 3.8 T magnetic field produced by the solenoid at this location, and resistant to the radiation levels expected in the EB over a ten year period. They also have high enough gain to counter to low light yield of the crystals. All of this makes them an ideal choice for use in the EB. Each APD has an active area of 5 × 5 mm² and are operated at a gain of 50 which requires a bias voltage between 340 and 430 V. As the gain of the APDs is highly dependent on the applied bias voltage and any gain instability would translate to degradation in energy resolution, very stable power supplies are used to maintain voltages within a few tens of mV.

The EE cover the pseudorapidity range 1.497 < | η | < 3.0. The crystals in the EE have a 28.62×28.62 mm² front face cross section and 30×30 mm² rear face cross section. Each crystal is 220 mm long which corresponds to 24.7 radiation lengths and are grouped in 5×5 units called supercrystals (SCs). Two halves, called *Dees*, make up each EE. Each Dee contains 138 SCs and 18 partial SCs which lie along the inner and outer circumference. On the back of each crystal in EE is a VPT which is a conventional photomultiplier with a single gain stage. While not as compact as the APDs used in the EB, the VPTs are a more suitable for the more hostile environment at higher η . Each VPT has a 25-mm diameter and approximately 280 mm² of active area. Though the VPT gain and quantum efficiency are lower than that of the APDs this is offset by the larger active area allowing for better light collection. Figure 4.6 shows the orientation of the crystals, modules, and supermodules within the ECAL. [7]

4.4.3 Preshower layer

In front of each EE is a preshower (ES) detector. The main purpose of the ES is to identify photons resulting from $\pi^0 \rightarrow \gamma\gamma$ within the pseudorapidity range $1.653 < |\eta| < 2.6$, but it also aids in the identification of electrons against minimum ionizing particles (MIPs) and provides a spacial resolution of 2 mm compared to the 3 mm resolution of the EB and EE. The ES acts as a two-layered sampling calorimeter. Lead radiators make up the first layer. These initiate electromagnetic showers from incoming electrons or photons. The deposited energy and transverse profiles of these showers are then measured by the silicon strip sensors which make up the second layer.

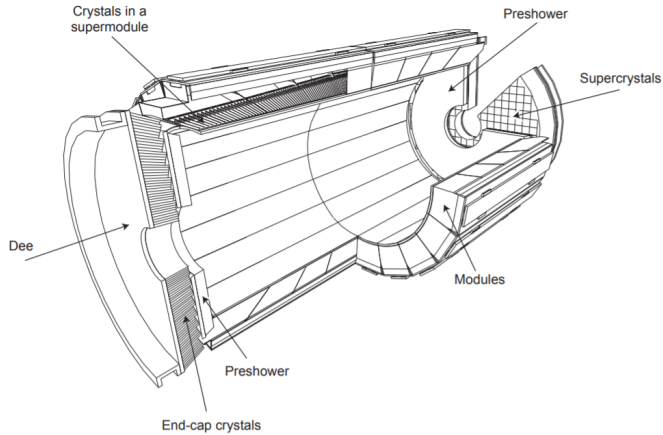


Fig. 4.6: Schematic of ECAL. Reprint from [7]

4.4.4 Performance

The energy resolution of the ECAL can be parameterized as

$$\frac{\sigma}{E} = \frac{S}{\sqrt{E}} \oplus \frac{N}{E} \oplus C \quad (4.4)$$

where S is the stochastic term characterizing the size of photostatistical fluctuations, N is the term characterizing the contributions of electronic, digital, and pileup noise, and C is a constant which accounts for crystal performance non-uniformity, intercalibration errors, and leakage of energy from the back of a crystal. The values for these terms, as measured in a beam test using 20 to 250 GeV electrons, are $S = 0.028 \text{ GeV}^{1/2}$, $N = 0.12 \text{ GeV}$, and $C = 0.003$. [7]

4.5 Hadronic Calorimeter

4.6 Muon System

5. MIP TIMING DETECTOR (MTD)

In the coming years the LHC will be working toward upgrades that will lead a substantial increase in luminosity. The timeline for future operations of the LHC is shown in Figure 5.1. In 2019 the LHC entered a two-year shutdown, Long Shutdown 2 (LS2). Upgrades of the LHC injector complex to increase the beam brightness will take place during this shutdown. After LS2 the LHC will enter Run 3 which will run for three years at 13-14 TeV. At the completion of Run 3 the LHC will enter Long Shutdown 3 (LS3) which will last approximately 2.5 years. During LS3 the optics in the interaction region will be upgraded to produce smaller beams at the interaction point. The completion of this upgrade will usher in the High Luminosity (HL-LHC) era or Phase 2 of LHC operations, during which the combination of brighter beams and a new focusing scheme at the IP allows for a potential luminosity of $2 \times 10^{35} \text{ cm}^{-2}\text{s}^{-1}$ at the beginning of each fill [1].

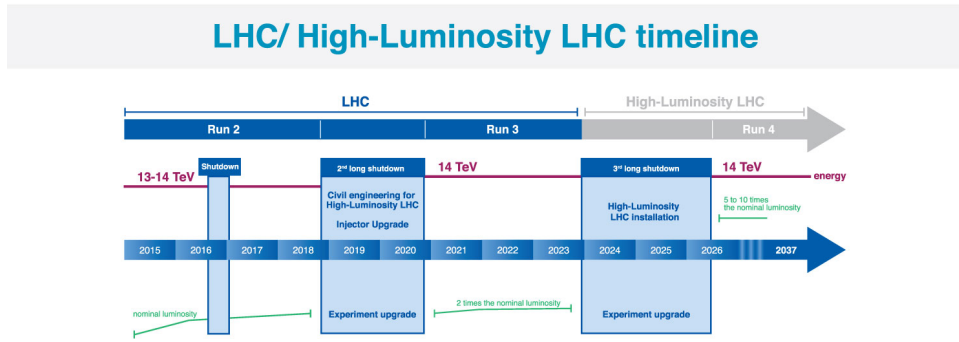


Fig. 5.1: Timeline for LHC [8]

The increased luminosity results in more interactions per bunch crossing or pileup. In order to limit the amount of pileup the experiments must disentangle to more manageable levels, the nominal scenario would be operating at a stable luminosity of $5.0 \times 10^{34} \text{ cm}^{-2} \text{ s}^{-1}$. This would limit the

pileup to an average of 140. The ultimate scenario for operations would be running at $7.5 \times 10^{34} \text{ cm}^{-2} \text{ s}^{-1}$ which brings the average pileup up to 200. The CMS detector in its current state is not capable of dealing with $\approx 140\text{-}200$ pileup. At this level of pileup the spacial overlaps of tracks and energy depositions would lead to a degradation in the ability to identify and reconstruct hard interactions. In order to preserve the data quality of the current CMS detector this increased pileup must be reduced to an equivalent level approximately equal to current LHC operations which is ~ 40 . The collision vertices within a bunch crossing have an RMS spread of 180-200 ps in time. If the beam spot were to be sliced into consecutive snap shots of 30-40 ps then the pileup levels per snapshot would be approximately 40. The space-time reconstruction of a 200 pileup event is shown in Figure 5.2. The addition of timing information to the z position spreads apart the vertices that would otherwise have been merged together and indiscernible. In order to achieve this a detector dedicated to the precise timing of minimum ionizing particles (MIPs), the MTD, will be added to the CMS detector.

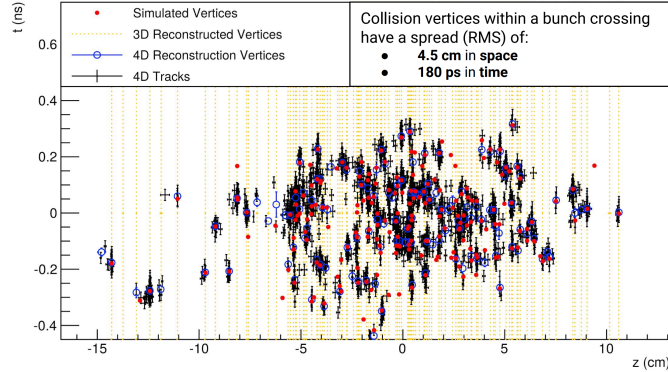


Fig. 5.2: Timelayer thingy

The MTD will provide timing information with a resolution of 30-40 ps at the start of the HL-LHC era. Radiation damage is expected to degrade this to 50-60 ps by the end of the HL-LHC era.

5.0.1 Barrel Timing Layer

The

BIBLIOGRAPHY

- [1] G. Apollinari, O. Brüning, T. Nakamoto, and Lucio Rossi. High Luminosity Large Hadron Collider HL-LHC. *CERN Yellow Rep.*, (5):1–19, 2015.
- [2] S Baird. Accelerators for pedestrians; rev. version. Technical Report AB-Note-2007-014. CERN-AB-Note-2007-014. PS-OP-Note-95-17-Rev-2. CERN-PS-OP-Note-95-17-Rev-2, CERN, Geneva, Feb 2007.
- [3] David Barney. CMS Slice. Feb 2015.
- [4] Jean-Luc Caron. Cross section of lhc dipole.. dipole lhc: coupe transversale. "AC Collection. Legacy of AC. Pictures from 1992 to 2002.", May 1998.
- [5] CMS Collaboration. CMS Technical Design Report for the Pixel Detector Upgrade. Technical Report CERN-LHCC-2012-016. CMS-TDR-11, Sep 2012. Additional contacts: Jeffrey Spalding, Fermilab, Jeffrey.Spalding@cern.ch Didier Contardo, Universite Claude Bernard-Lyon I, didier.claude.contardo@cern.ch.
- [6] CMS Collaboration. Description and performance of track and primary-vertex reconstruction with the CMS tracker. *JINST*, 9(CMS-TRK-11-001. CERN-PH-EP-2014-070. CMS-TRK-11-001):P10009. 80 p, May 2014. Comments: Replaced with published version. Added journal reference and DOI.
- [7] The CMS Collaboration. The CMS experiment at the CERN LHC. *Journal of Instrumentation*, 3(08):S08004–S08004, aug 2008.
- [8] Cinzia De Melis. Timeline for the LHC and High-Luminosity LHC. Frise chronologique du LHC et du LHC haute luminosité. Oct 2015. General Photo.
- [9] Lyndon Evans and Philip Bryant. LHC machine. *Journal of Instrumentation*, 3(08):S08001–S08001, aug 2008.

- [10] Tai Sakuma and Thomas McCauley. Detector and event visualization with SketchUp at the CMS experiment. *Journal of Physics: Conference Series*, 513(2):022032, jun 2014.